NEW IDEA TO PROBE PROPERTIES OF QUARK–GLUON JETS AT THE LHC*

Petr Baroň

Institute of Nuclear Physics Polish Academy of Sciences
Radzikowskiego 152, 31-342 Kraków, Poland
Petr.Baron@ifj.edu.pl

Michael H. Seymour

Lancaster-Manchester-Sheffield Consortium for Fundamental Physics
Department of Physics and Astronomy, University of Manchester, M13 9PL, U.K.
Michael.Seymour@manchester.ac.uk

Andrzej Siódmok

Jagiellonian University, Łojasiewicza 11, 30-348 Kraków, Poland
Andrzej.Siodmok@uj.edu.pl

Received 10 May 2024, accepted 19 June 2024, published online 5 August 2024

This paper provides a cross-check of a novel method for measuring quark- and gluon-jet properties at the Large Hadron Collider (LHC). The method relies on data of dijet events collected at two different centre-of-mass energies of LHC operation. By combining these two datasets each with a different abundance of gluon jets, the jet properties categorized into quark and gluon distributions are obtained on a statistical basis. The cross-check of derived quark and gluon distributions is performed against "truth" distributions obtained by matching jet to parton using the minimal difference in rapidity-azimuth distance $\Delta R(\mathrm{jet}, \mathrm{parton})$.

DOI:10.5506/APhysPolBSupp.17.5-A35

1. Introduction

Differentiating quark jets from gluon jets increases the sensitivity of studies searching for beyond the Standard Model (BSM) physics, as BSM signals are often dominated by quarks while Standard Model backgrounds are dominated by gluons. The aim of this method [1] is to separate quark- and

* Presented by P. Baroň at the 30$^{\mathrm{th}}$ Cracow Epiphany Conference on *Precision Physics at High Energy Colliders*, Cracow, Poland, 8–12 January, 2024.

gluon-jet samples on a statistical basis without need for an independent event-by-event tag. The strategy involves constructing observables from ratios of physical quantities measured at different energies. This approach minimizes the impact of systematic errors, making the measurements more robust and reliable. The method can be applied using the existing Large Hadron Collider (LHC) data collected at different energies, making it a practical and cost-effective way to enhance current and future analyses without requiring additional special runs of the LHC.

The novelty of the method originates in using two datasets of dijet events collected at distinct centre-of-mass energies while keeping the same kinematic cuts and detector parameters to reduce systematic uncertainties and avoiding kinematic bias (*e.g.* high-p_{T} quark jet radiates similarly as low-p_{T} gluon jet). The dataset collected at higher centre-of-mass energy has a larger portion of gluon jets, as can be seen in figure 2 (a). Within both collected datasets, the generalised angularities [2]

— multiplicity — λ_0^0,

— p_{T}^D — λ_0^2,

— LHA — $\lambda_{0.5}^1$,

— width — λ_1^1, and

— mass — λ_2^1

were calculated

$$\lambda_\beta^\kappa = \sum_{i \in \mathrm{jet}} z_i^\kappa \theta_i^\beta \,, \tag{1}$$

where i represents the jet constituent, z_i is the transverse momentum fraction of the jet constituent $z_i \equiv \frac{p_{\mathrm{T}i}}{\sum_{j\in \mathrm{jet}} p_{\mathrm{T}j}} \in [0,1]$, and $\theta_i \equiv \frac{R_{i\hat{n}}}{R} \in [0,1]$ is given using $R_{i\hat{n}}$, the rapidity-azimuth distance to the jet axis, and R is the jet-radius parameter. Having jet angularites from both datasets collected at different energies enables to derive quark and gluon angularities, which can potentially differentiate quark jets from gluon jets on a statistical basis. The method of derivation of quark and gluon angularities is described in Section 3. As a cross-check of this method, jets are tagged as quark or gluon based on the closest parton in the rapidity-azimuth distance $\Delta R(\mathrm{jet}, \mathrm{parton})$. From these tagged jets, the quark and gluon angularity distributions, labelled "truth" distributions, were calculated and compared against those derived by the presented method.

2. Event selection

The jets from dijet events $pp \to jj$ were generated using event generators Herwig 7.2.2 [3, 4] (MMHT2014lo68cl PDF set [5]) and PYTHIA 8.240 [6, 7] (NNPDF2.3 QCD+QED LO PDF set [8]) at four different centre-of-mass energies $\sqrt{s} = 900$ GeV, 2.36 TeV, 7 TeV, and 13 TeV simulating the LHC runs. For simplicity, Section 3 explains the method using two of these energies, but the result plots are presented using all four listed energies. The anti-k_{T} algorithm [9] implemented in the FastJet package [10, 11] with radii $R = 0.2$, 0.4, 0.6, 0.8, and 1.0 was used for jet reconstruction. Transverse momentum p_{T} cuts on the jets were applied

$$p_{\mathrm{T\,sublead}}/p_{\mathrm{T\,lead}} > 0.8 \tag{2}$$

and

$$(p_{\mathrm{T\,lead}} + p_{\mathrm{T\,sublead}})/2 > p_{\mathrm{T}}^{\mathrm{cut}}\,, \tag{3}$$

where $p_{\mathrm{T\,lead}}$ and $p_{\mathrm{T\,sublead}}$ is the transverse momentum of the leading, and subleading jet respectively. Four transverse momentum cuts $p_{\mathrm{T}}^{\mathrm{cut}} = 50$, 100, 200, and 400 GeV were taken into account. Also the impact of jet trimming (see *e.g.* [12–15]) was tested by applying a modified mass drop tagger (MMDT) with $\mu = 1$ [12, 16] (equivalently, soft drop declustering with $\beta = 0$ [17]) and $z_{\mathrm{cut}} = 0.1$.

3. Quark and gluon angularities

Five types of angularities were calculated according to equation (1) at different $\sqrt{s} = 0.9$, 2.36, 7, and 13 TeV. For example, in figure 1, the jet angularities λ_0^0 (multiplicities, $R = 0.4$, $p_{\mathrm{T}}^{\mathrm{cut}} = 100$ GeV) are plotted by green dashed line — 900 GeV and by black line — 13 TeV. Each distribution λ_0^0 at the energies 900 GeV and 13 TeV obtains different portions of quark and gluon jets

$$\lambda = f\lambda_g + (1-f)\lambda_q\,, \tag{4}$$

where f is the fraction of gluon jets, $(1-f)$ fraction of quark jets, λ_g gluon angularity, and λ_q quark angularity. To obtain quark λ_q and gluon λ_g angularities, the idea is to use jet angularities derived (or ideally measured) at two energies. Without loss of generality with respect to the example in figure 1, the equations take the form of

$$\lambda^{900} = f^{900}\lambda_g + \left(1-f^{900}\right)\lambda_q\,, \tag{5}$$

$$\lambda^{13000} = f^{13000}\lambda_g + \left(1-f^{13000}\right)\lambda_q\,, \tag{6}$$

where the upper script refers to the two energies 900 GeV and 13 TeV. Assuming that quark λ_q and gluon λ_q angularities are independent of the energy, one can extract the quark angularity λ_q as

$$\lambda_q = \frac{f^{13000}\lambda^{900} - f^{900}\lambda^{13000}}{f^{13000} - f^{900}}, \tag{7}$$

and the gluon angularity λ_g as

$$\lambda_g = \frac{\left(1 - f^{900}\right)\lambda^{13000} - \left(1 - f^{13000}\right)\lambda^{900}}{f^{13000} - f^{900}}. \tag{8}$$

The coefficients f^{900} and f^{13000} are set by simulation and will be discussed in Section 4. The resulting quark λ_q (red/light grey) and gluon λ_g (blue/grey) angularities (multiplicities) are plotted in figure 1. Expressing equations (7) and (8) for general choice of energies s_1 and s_2 gives

$$\lambda_q = \frac{f^{s_1}\lambda^{s_2} - f^{s_2}\lambda^{s_1}}{f^{s_1} - f^{s_2}} \tag{9}$$

and

$$\lambda_g = \frac{\left(1 - f^{s_2}\right)\lambda^{s_1} - \left(1 - f^{s_1}\right)\lambda^{s_2}}{f^{s_1} - f^{s_2}}. \tag{10}$$

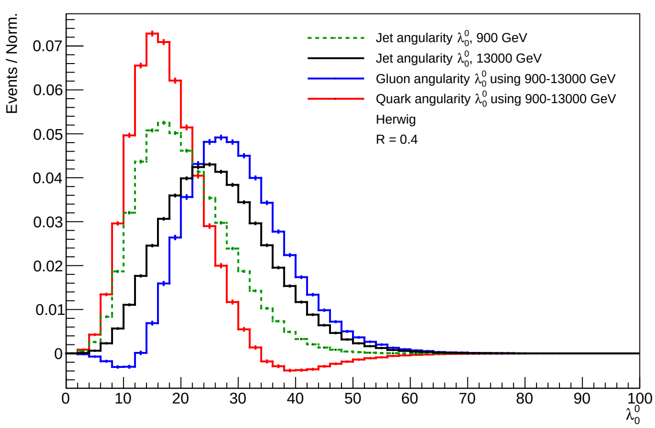

Fig. 1. (Colour on-line) Derived distributions of quark and gluon angularity (multiplicity) λ_q (red/light grey line) and λ_g (blue/grey line) as linear combinations of those measured at different energies (green dashed line and black line). Figure taken from [1].

4. Gluon fraction coefficients f^{s_1} and f^{s_2}

While hadronization and parton showering are being switched off in the Monte Carlo generators Herwig 7 and PYTHIA 8, the gluon fraction was defined as a function of p_{T}

$$f(p_{\mathrm{T}}) = \frac{N_{\mathrm{gluons}}(p_{\mathrm{T}})}{N_{\mathrm{gluons}}(p_{\mathrm{T}}) + N_{\mathrm{quarks}}(p_{\mathrm{T}})}\,, \tag{11}$$

where N is the number of partons (quarks or gluons). In figure 2 (a) the examples of gluon fractions as a function of transverse momentum $f(p_{\mathrm{T}})$ at $\sqrt{s} = 900$ GeV and 13000 GeV of Herwig (solid lines) are showed. In figure 2 (b), the p_{T} distributions of jets ($R = 0.4$) that passed the event selection cuts obtained by running a Monte Carlo simulation (including hadronization and parton shower) at two different collision energies 900 and 13000 GeV are shown. The mean $\langle p_{\mathrm{T}} \rangle$ of the jet distribution for the two energies are as follows:

— jet p_{T} ($\sqrt{s} = 900$ GeV) $\rightarrow \langle p_{\mathrm{T}} \rangle = 114.57$ GeV,

— jet p_{T} ($\sqrt{s} = 13$ TeV) $\rightarrow \langle p_{\mathrm{T}} \rangle = 125.63$ GeV.

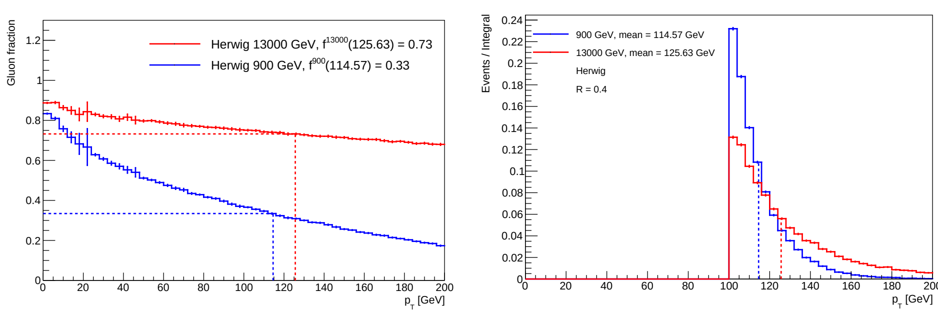

(a) (b)

Fig. 2. (Colour on-line) (a) gluon fractions obtained using equation (11) from Herwig's simulation of proton–proton dijet process without hadronization and parton showering at $\sqrt{s} = 900$ GeV f^{900} (blue/black solid line) and $\sqrt{s} = 13000$ GeV f^{13000} (red/grey solid line). Dashed lines show the chosen values f^{900} and f^{13000} for the point at the mean of the jet p_{T} distributions. (b) Normalised transverse momentum of the leading and subleading jets at energy 900 and 13000 GeV. Dashed lines represent the mean of the distributions used to evaluate the coefficients of the gluon fraction. Figures taken from [1].

The scaling coefficients f^{900} and f^{13000}, as illustrated by the dashed lines in Fig. 2 (a), are obtained using the gluon fractions at the point of $\langle p_{\mathrm{T}} \rangle$

$$f^{900} = f^{900}(\langle p_{\mathrm{T}} \rangle) = f^{900}(114.57\ \mathrm{GeV}) = 0.33\,, \tag{12}$$

$$f^{13000} = f^{13000}(\langle p_{\mathrm{T}} \rangle) = f^{13000}(125.63\ \mathrm{GeV}) = 0.73\,. \tag{13}$$

5. Results

Figure 3 (a) shows the multiplicities λ_0^0 ($R = 0.4$, $p_{\mathrm{T}}^{\mathrm{cut}} = 100$ GeV) of the quark jets (red/light grey lines) and the gluon jets (blue/dark grey lines). The plot includes angularities derived using all 6 energy combinations which are denoted by various types of lines. The dots represent the angularities derived with the Multiple-Parton Interactions model (MPI) and Parton Shower Initial-State Radiation (ISR) being switched off. In order to simplify such a plot in figure 3 (a), figure 3 (b) shows the same observable, solid lines representing the averaged quark and gluon angularities across different energy combinations. The filled area builds the envelope of the different energy combinations and the ticks represent the envelope of the statistical uncertainties of the angularities. This averaged plot gives insight into how the observables are robust to systematic effects.

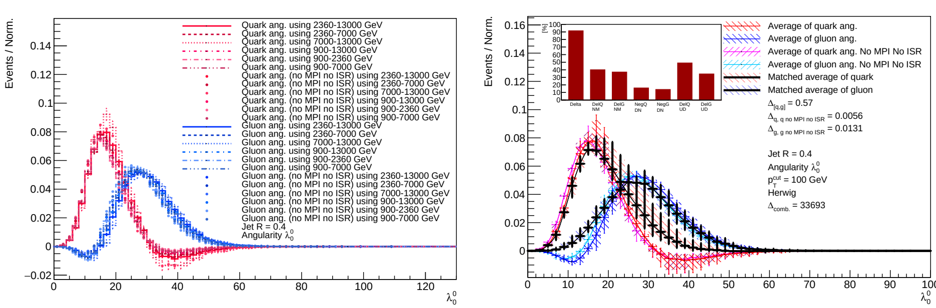

(a) (b)

Fig. 3. (a) Quark and gluon multiplicities λ_0^0 ($R = 0.4$, $p_{\mathrm{T}}^{\mathrm{cut}} = 100$ GeV) for all six energy combinations, (b) averaged plot showing the envelopes of the different energy combinations as filled areas and their statistical uncertainties as ticks (below). Figures taken from [1].

The results are summerized by figures 4 (a)–(e) which represent the best selection based on the Δ_{comb} score [1] for each type of angularity. The score accounts for high separation power between quark and gluon angularities, low negativity, robustness to MPI and ISR effects, and energy independence of the angularities. On top of that, the thick solid black lines indicate truth quark and gluon distributions obtained by matching to partons using minimal ΔR.

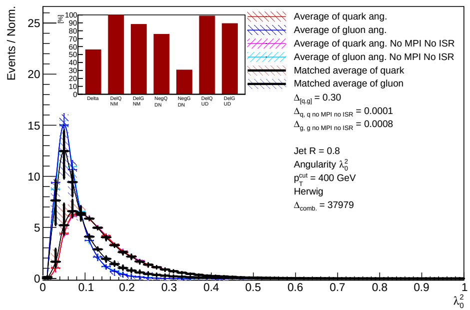

(a) p_{T}^{D} λ_0^2, $R = 0.8$, $p_{\mathrm{T}}^{\mathrm{cut}} = 400$ GeV

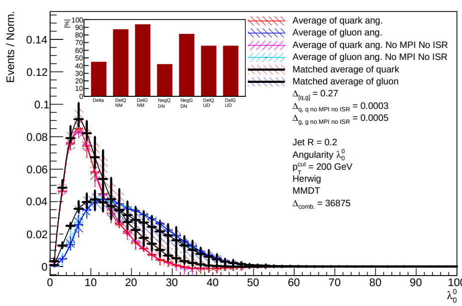

(b) Mult. λ_0^0, $R = 0.2$, $p_{\mathrm{T}}^{\mathrm{cut}} = 200$ GeV

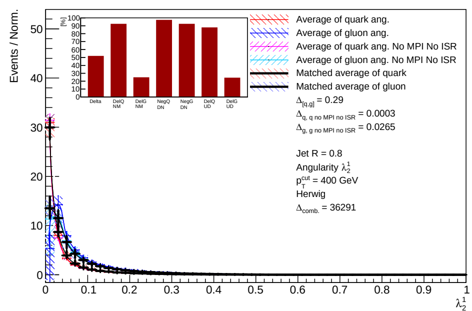

(c) Mass λ_2^1, $R = 0.8$, $p_{\mathrm{T}}^{\mathrm{cut}} = 400$ GeV

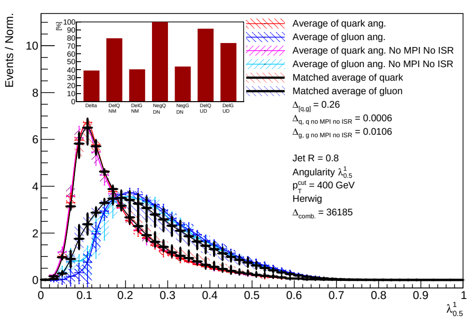

(d) LHA $\lambda_{0.5}^1$, $R = 0.8$, $p_{\mathrm{T}}^{\mathrm{cut}} = 400$ GeV

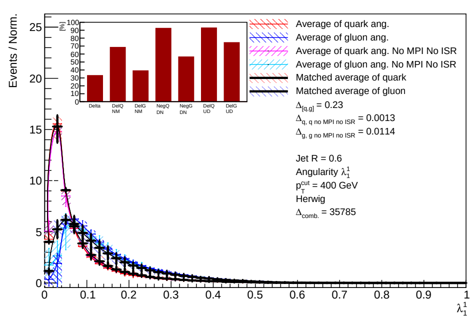

(e) Width λ_1^1, $R = 0.6$, $p_{\mathrm{T}}^{\mathrm{cut}} = 400$ GeV

Fig. 4. (Colour on-line) Quark and gluon averaged angularities derived using Herwig event generator, using the average of 6 energy combinations 900–2360, 900–7000, 900–13000, 2360–7000, 2360–13000, and 7000–13000 GeV. The thick black solid lines indicate truth quark and gluon angularities obtained by matching to partons using minimal ΔR. Figures taken from [1].

6. Conclusion

The best-performing angularities presented in plots 4 (a)–(e) support the assumption that, for these angularities, quarks and gluons remain independent of collision energy. This conclusion is drawn from the relatively small uncertainties, which represents angularities derived at different energy combinations. The truth distributions are in agreement within uncertainties in the case of quark angularities, while gluon truth angularities are slightly shifted out of the uncertainty band in a few bins. The study demonstrates that it is feasible to perform measurements based on the proposed method at the LHC at energies of 7 TeV and 13 TeV.

M.H.S. gratefully acknowledges funding from the U.K. Science and Technology Facilities Council (grant No. ST/T001038/1). The work of A.S. and P.B. is funded by grant No. 2019/34/E/ST2/00457 of the National Science Centre (NCN), Poland. P.B. is also supported by the Priority Research Area Digiworld under the program Excellence Initiative — Research University at the Jagiellonian University in Kraków and by the Polish National Agency for Academic Exchange NAWA under the Programme STER Internationalisation of doctoral schools, project No. PPI/STE/2020/1/00020.

REFERENCES

[1] P. Baroň, M.H. Seymour, A. Siódmok, *Eur. Phys. J. C* **84**, 28 (2024), arXiv:2307.15378 [hep-ph].

[2] A.J. Larkoski, J. Thaler, W.J. Waalewijn, *J. High Energy Phys.* **2014**, 129 (2014), arXiv:1408.3122 [hep-ph].

[3] J. Bellm *et al.*, *Eur. Phys. J. C* **76**, 196 (2016), arXiv:1512.01178 [hep-ph].

[4] J. Bellm *et al.*, *Eur. Phys. J. C* **80**, 452 (2020), arXiv:1912.06509 [hep-ph].

[5] L.A. Harland-Lang, A.D. Martin, P. Motylinski, R.S. Thorne, *Eur. Phys. J. C* **75**, 204 (2015), arXiv:1412.3989 [hep-ph].

[6] T. Sjöstrand *et al.*, *Comput. Phys. Commun.* **191**, 159 (2015), arXiv:1410.3012 [hep-ph].

[7] C. Bierlich *et al.*, *SciPost Phys. Codeb.* **2022**, 8 (2022), arXiv:2203.11601 [hep-ph].

[8] NNPDF Collaboration (R.D. Ball *et al.*), *Nucl. Phys. B* **877**, 290 (2013), arXiv:1308.0598 [hep-ph].

[9] M. Cacciari, G.P. Salam, G. Soyez, *J. High Energy Phys.* **2008**, 063 (2008), arXiv:0802.1189 [hep-ph].

[10] M. Cacciari, G.P. Salam, *Phys. Lett. B* **641**, 57 (2006), arXiv:hep-ph/0512210.

[11] M. Cacciari, G.P. Salam, G. Soyez, *Eur. Phys. J. C* **72**, 1896 (2012), arXiv:1111.6097 [hep-ph].

[12] J.M. Butterworth, A.R. Davison, M. Rubin, G.P. Salam, *Phys. Rev. Lett.* **100**, 242001 (2008), arXiv:0802.2470 [hep-ph].

[13] S.D. Ellis, C.K. Vermilion, J.R. Walsh, *Phys. Rev. D* **80**, 051501 (2009), arXiv:0903.5081 [hep-ph].

[14] S.D. Ellis, C.K. Vermilion, J.R. Walsh, *Phys. Rev. D* **81**, 094023 (2010), arXiv:0912.0033 [hep-ph].

[15] D. Krohn, J. Thaler, L.-T. Wang, *J. High Energy Phys.* **2010**, 084 (2010), arXiv:0912.1342 [hep-ph].

[16] M. Dasgupta, A. Fregoso, S. Marzani, G.P. Salam, *J. High Energy Phys.* **2013**, 029 (2013), arXiv:1307.0007 [hep-ph].

[17] A.J. Larkoski, S. Marzani, G. Soyez, J. Thaler, *J. High Energy Phys.* **2014**, 146 (2014), arXiv:1402.2657 [hep-ph].